Multichannel photon counting instrument for spatially resolved near infrared spectroscopy

Vasilis Ntziachristos[a)]
Department of Bioengineering, University of Pennsylvania, Philadelphia, Pennsylvania 19104-6089

XuHui Ma
Department of Biochemistry/Biophysics, University of Pennsylvania, Philadelphia, Pennsylvania 19104-6089

A. G. Yodh
Department of Physics and Astronomy, University of Pennsylvania, Philadelphia, Pennsylvania 19104-6089

Britton Chance
Department of Biochemistry/Biophysics, University of Pennsylvania, Philadelphia, Pennsylvania 19104-6089

(Received 4 August 1998; accepted for publication 20 October 1998)

We have developed a multichannel photon counting instrument for near infrared spatially resolved spectroscopy. The instrument uses two laser diodes at 780 and 830 nm. The two wavelengths are time multiplexed at a rate of 5 MHz for virtually simultaneous measurements at the two wavelengths. The photon pulses are then multiplexed with an optical switch so that the incident optical signals are directed to different source positions. Eight time-correlated channels have been employed for simultaneous acquisition of spectroscopic data at multiple locations. Photon detection is performed by multichannel plate photomultiplier tubes. Robust and accurate data analysis tools to perform deconvolution, data fitting, and absorption change quantification are presented. The instrument has been tested with phantoms simulating tissue optical properties. Absolute optical properties, namely absorption and reduced scattering coefficient, have been determined with an accuracy of $\pm 5\%$. Quantification of absorption changes can be achieved with an accuracy of 10^{-3} cm^{-1} and a sensitivity of the order of 10^{-4} cm^{-1}. Finally spatially resolved measurements of primary motor-cortex activation have been performed and successfully coregistered with functional magnetic resonance imaging data. © *1999 American Institute of Physics.*
[S0034-6748(99)04001-0]

I. INTRODUCTION

Near infrared (NIR) spectroscopy of tissue is an important noninvasive monitor for measurement of tissue absorption and scattering, and for extraction of the concentrations of tissue chromophores such as oxygenated and deoxygenated hemoglobin,[1,2] cytochrome oxidase,[3] and water.[4] Measurements of physiologically important parameters such as blood volume and oxygenation,[5–8] can further be related to metabolic activity,[9,10] functional activity,[11] or presence of disease.[12] NIR spectroscopic measurements have also been used to determine tissue fat composition[13] and blood glucose levels.[14] The most popular wavelength range lies in the 750–850 nm spectral window where the relatively low tissue absorption enables deep light penetration.

Three major experimental techniques exist in the field of NIR spectroscopy. The simplest is continuous wave spectroscopy where light of constant intensity is injected into the tissue, and then the attenuated light signal, due to tissue absorption and scattering, is measured at some distance from the source.[15,16] A more elaborate approach is the intensity modulation method where the light source intensity is modulated at single or multiple frequencies.[1,17,18] The detection system in this case consists of a demodulator, which resolves the amplitude and the phase shift of the detected light, relative to the incident light, as a function of the source-detector separation. The third approach, the time-resolved technique,[1,19] uses short pulses of light injected into the tissue. The detection process requires a time-correlated photon counting system, which makes a histogram of the number of photons arriving as a function of time. This measurement is used to calculate the distribution of photon paths in tissue and relate them to tissue absorption and scattering. Of the three methods, the time-resolved technique contains the highest information content per source detector pair, compared only with the multifrequency intensity modulation method.

We have developed a multichannel single photon counting instrument, based on the time-resolved technique, that employs parallel signal detection. The major components of the instrument are similar to the imager we have developed for breast cancer detection applications.[20] Modifications have been implemented in the optics of the source, detector, and tissue interface enabling better impulse response characteristics. In this article we focus on the design and utilization of this instrument for spatially resolved *spectroscopic* applications. We discuss the calculation tools we are using for spectroscopy and evaluate the performance of the instrument on tissue phantoms. A robust deconvolution-fitting algorithm,

a)Electronic mail: vasilis@mail.med.upenn.edu

for calculation of absolute absorption and reduced scattering coefficients, is presented. A novel algorithm for very accurate measurement of absorption differences is introduced. Sources of errors are identified and accuracy limits are derived. Finally NIR spatially resolved spectroscopic measurements are obtained *in vivo* during contralateral primary motor cortex activation of a human volunteer. The results show excellent coregistration with functional magnetic resonance.

II. THEORY AND DATA ANALYSIS

A. Light diffusion

The diffusive nature of light propagation in highly scattering, low absorbing homogeneous media, has been well studied and is described by the diffusion equation,[19,21] i.e.,

$$\frac{1}{c}\frac{\partial}{\partial t}u(r,t)-D\nabla^2 u(r,t)+\mu_a u(r,t)=S(r,t), \tag{1}$$

where $u(r,t)$ is the photon fluence [J cm^{-2} s^{-1}] at a position r from the source at time t, c is the speed of light into the medium [cm s^{-1}], $D=1/3(\mu_s'+\mu_a)$ [cm] is the diffusion coefficient for a highly scattering, low absorbing medium, μ_s' the reduced scattering coefficient [cm^{-1}], μ_a the absorption coefficient [cm^{-1}], and $S(r,t)$ a source term [J cm^{-3} s^{-1}]. The solution of this equation for an isotropic point source, $S(r,t)=A\,\delta(t=0,r=0)$, in an infinite medium, is given by

$$u(r,t)=Ac(4\pi Dct)^{-3/2}\exp\left(-\frac{r^2}{4Dct}-\mu_a ct\right). \tag{2}$$

Here A is a dimensionless scaling term that accounts for the effects of the laser source strength and the detector gain. The quantity actual detected by a photosensor is the directional photon current $J(r,t)$ [J cm^{-2} s^{-1}], which is related to the photon fluence via Fick's law

$$J(r,t)=-D\nabla u(r,t)=A(4\pi Dc)^{-3/2}t^{-5/2}\frac{r}{2}\times\exp\left(-\frac{r^2}{4Dct}-\mu_a ct\right). \tag{3}$$

By fitting time-resolved measurements to solutions of the time-dependent diffusion equation for semi-infinite (reflectance) or slab (transmittance) geometries[19] we obtain the average absorption and scattering properties of the sample. In tissues, light absorption and scattering properties at multiple wavelengths can be related to blood volume and oxygenation.[1] The accuracy of these properties depends on the degree to which the tissues are homogeneous and satisfy the actual boundary conditions employed in calculations.

B. Deconvolution and data fitting

As a result of the finite duration of the laser photon pulses, the photon dispersion along the fibers and the photoelectron spreading in the detector, the measured signal $s(t)$ is a convolution of a ''real'' signal $r(t)$ and the finite impulse response of the instrument $h(t)$, i.e.,

$$s(t)=h(t)\otimes r(t)=\int_{-\infty}^{\infty}h(t-\nu)r(\nu)\,d\nu. \tag{4}$$

In order to obtain absolute tissue optical properties we need to correct for instrumental response. The simplest deconvolution operation is the linear frequency domain method that takes advantage of the simplicity of the convolution theorem

$$R(f)=\frac{S(f)}{H(f)}, \tag{5}$$

where $R(f)$, $S(f)$, and $H(f)$ are the Fourier transforms of the signals $r(t)$, $s(t)$, and $h(t)$, respectively. The inverse Fourier transform of $R(f)$ yields the desired $r(t)$ signal. Unfortunately, except in certain cases where extremely favorable signal-to-noise ratios are available, the inverse Fourier transform of Eq. (5) is severely degraded by measurement noise even when matched filtering is performed.[22]

Under these circumstances improved behavior can be obtained by numerical methods in the time domain. Jannson[22,23] has suggested an efficient and accurate iterative technique, which is a modification on an original suggestion by Van Cittert[24] given by

$$r_n=r_{n-1}+a(r_{n-1})(s-r_{n-1}\otimes h), \tag{6}$$

where the subscript n denotes the iteration step. The time dependence $r(t)$, $s(t)$, and $h(t)$ is implied but not explicitly written. The first guess for r is typically s. Both conversion time and accuracy depend on the selection of the quantity a, which depends on the amplitude of r_{n-1}, is assigned empirically,[22] and is application specific. Proper a structure helps eliminate nonphysical solutions produced by the linear Van Cittert method (where a equals 1). One of the great advantages of these linear and nonlinear numerical methods is that they convert a deconvolution to a convolution operation. Convolution is an easily manipulated operation, and in the case of the linear methods it acts as a low pass filter reducing noise. Equation (6) however requires careful implementation to ensure convergence and optimum results. The deconvolved result, after n iterations, can be fitted with the solution of the diffusion equation that best represents the boundary conditions of the measurement. Other deconvolution methods based on the maximum likelihood estimates of the spectra have also been proposed.[25,26] The existence of a large number of deconvolution methods exemplifies the complexity of the operation and the need for application specific algorithms to ensure best performance.

In this article we discuss an algorithm that we have found to have superior convergence characteristics compared to Eq. (6). The algorithm performs fitting and deconvolution simultaneously, offering time efficiency and implementation simplicity. It is based on the general observation that in order to resolve tissue optical properties we need to find the parameters of a *model function* $y(t)$ that will produce an output that most closely matches our data. However here, instead of deconvolving the true time-resolved curve $y(t)$ from the measured signal $s(t)$ and then fitting the deconvolved curve, we convolve the instrument impulse response $h(t)$ with various model functions for $y(t)$ trying to match the convolution

result to $s(t)$ in the least square sense. In the general case the model function can be dependent on a number of parameters $a_1 \ldots a_M$. For our application the model function would be Eq. (3) for measurements of infinite homogeneous media or any solution of Eq. (1) that approximates our real measurement scheme. The parameters $a_1 \ldots a_M$ in our case are the absorption coefficient $\mu_{a,}$, the reduced scattering coefficient μ_s', the scaling factor A, the initial time t_0 and the separation r, or any subset of them depending on the availability of prior knowledge. The initial time t_0 is the time that the maximum of the finite-width laser photon pulse was launched into the medium. Thus $y(t)$ is

$$y(t)=y(t;\mu_a,\mu_s',A,t_0,r). \tag{7}$$

We define now a new model function $y^*(t)$ as the convolution of the model function $y(t)$ with the instrument impulse response $h(t)$, i.e.,

$$y^*(t)=h(t)\otimes y(t). \tag{8}$$

Then we use a nonlinear Levenberg–Marquardt fitting procedure[28] to minimize the χ^2 merit function[27]

$$\chi^2=\sum_{k=1}^{K}\left(\frac{s(k)-y^*(k)}{\sigma_k}\right)^2, \tag{9}$$

where k is the discrete time variable, K is the number of data points, and $\sigma_k=\sqrt{s(k)}$ is the measurement error (standard deviation) of the kth data point.

Equation (9) converts a two step deconvolution-fitting algorithm to a single step algorithm by performing an extra convolution step per fitting iteration. Therefore using this method we avoid the iterative step described by Eq. (6) and reduce the total data analysis time. Thus deconvolution is again converted to a convolution step for optimum behavior with noisy data. Convolution is performed in the frequency domain to increase calculation speed. Another advantage of Eq. (9) is that it does not require the empirical assignment of the function $a(r_{n-1})$ that Eq. (6) requires. This significantly simplifies the algorithm implementation and improves the robustness and accuracy of the method, ensuring convergence in a least-squares sense, even in very unfavorable signal-to-noise conditions. We have found that the use of Eq. (9) affords a superior approach in calculating absolute optical properties for NIR spectroscopy.

C. Quantification of absorption changes

Equation (9) is generally used for calculating absolute absorption and reduced scattering coefficients. However when considering absorption *changes* that might arise, for example as a function of time, we have found a new approach, which significantly outperforms in accuracy and sensitivity the method presented in the preceding section. Let us consider a small absorption change of the tissue volume from μ_{a1} to μ_{a2}, assuming constant reduced scattering coefficient μ_s'. Then the photon current will in general change from J_1 to J_2, respectively. For example if the medium is homogeneous and infinite, then for a source detector pair having a separation r

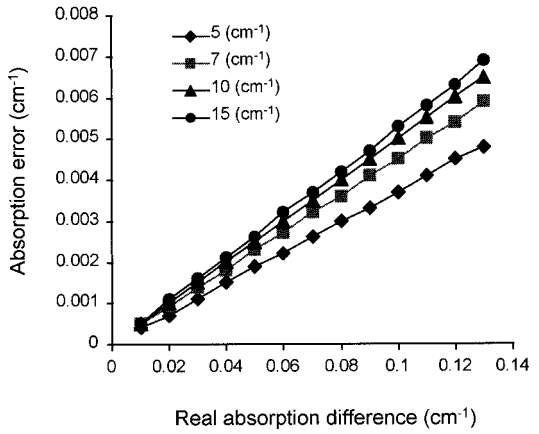

FIG. 1. Error for the quantification of absorption changes algorithm on simulated data as a function of the assumed real absorption change. The error of the method is of the order of 10^{-3} cm^{-1} for absorption changes below 0.02 cm^{-1}. For larger absorption changes the error deteriorates but remains below 10^{-2} cm^{-1} even for changes that rarely occur as a result of physiological responses. The error has a linear response with absorption change and hence may be easily corrected. The four curves plotted correspond to different background reduced scattering coefficients.

$$\frac{J_2(r,t)}{J_1(r,t)}=\exp[-(\mu_{a2}-\mu_{a1})ct]=\exp(-\Delta\mu_a ct). \tag{10}$$

Taking the natural logarithm of Eq. (10) and integrating over time retrieves the absorption change

$$\Delta\mu_a=-\frac{2}{c(t_2^2-t_1^2)}\int_{t_1}^{t_2}\ln\frac{J_2(r,t)}{J_1(r,t)}\,dt. \tag{11}$$

Here t_1 and t_2 can be any time interval within the pulse. Similarly the photon current for reflectance geometry is[19]

$$R(r,t)=(4\pi Dc)^{-3/2}z_0 t^{-5/2}\frac{r}{2}\exp\left(-\frac{r^2+z_0^2}{4Dct}\right)\times\exp(-\mu_a ct), \tag{12}$$

where $z_0=1/\mu_s'$. The ratio of reflected currents R_1 and R_2 gives again

$$\Delta\mu_a=-\frac{2}{c(t_2^2-t_1^2)}\int_{t_1}^{t_2}\ln\frac{R_2(r,t)}{R_1(r,t)}\,dt. \tag{13}$$

It is straightforward to show that even in more complex formulations, such as in reflectance using the extrapolated boundary condition,[29,30] or in transmittance with finite slab geometry, Eq. (13) still holds.

We have used this approach as a very sensitive and accurate analysis method for measurement of absorption changes. The main assumptions of the method are the postulation of invariable reduced scattering coefficient and that small absorption changes occur during the measurement. However, no knowledge of the exact reduced background scattering coefficient is required. Figure 1 shows the error as a function of absorption changes for different values of background reduced scattering coefficient. These simulated absorption changes were obtained using Eq. (13) and the error of the approximation was calculated by comparing the introduced absorption change with the absorption changes as calculated using Eq. (13). The error of the method is shown to

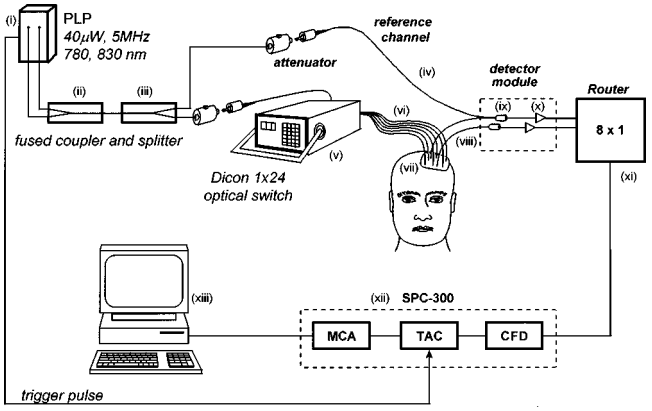

FIG. 2. Block diagram of the instrument. The main components are: (i) the laser source, (ii) the wavelength coupler, (iii) the 95/5 beam splitter, (iv) the reference branch, (v) the 1×9 optical switch, (vi) delivery optic fibers, (vii) fiber holder, (viii) collection fiber optic bundles, (ix) light detectors, (x) amplification unit, (xi) router, (xii) photon counting unit with multichannel pulse height analyzer (MCA), and finally (xiii) an Intel Pentium based personal computer for the control of the acquisition and data storage and analysis.

be quite insensitive to the exact value of the background reduced scattering coefficient. The error remains in most cases below 10^{-3} cm^{-1} for absorption coefficient changes of $\Delta\mu_a < 0.02$ cm^{-1} due to the small dependence of the diffusion coefficient to absorption. Furthermore it scales approximately linearly with the absorption change which enables easy error correction if higher absorption changes are monitored. Therefore the method can yield accurate results when only absorption changes are considered, even if a rough approximation of the background scattering is used.

Experimentally we have demonstrated that this method attains sensitivity to absorption changes of the order of 10^{-4} cm^{-1}. This is discussed in Sec. IV. This method is of essential importance for calculation of small absorption changes as in the case of brain functional activity measurements.[11]

III. APPARATUS

Figure 2 depicts the block diagram of the instrument, shown here applied to human brain measurement. The main components are: (i) the laser source, (ii) the wavelength coupler, (iii) the 95/5 beam splitter, (iv) the reference branch, (v) the 1×9 optical switch, (vi) delivery optic fibers, (vii) measurement pad, (viii) collection fiber optic bundles, (ix) light detectors, (x) amplification unit, (xi) router, (xii) photon counting unit with multichannel pulse height analyzer (MCA), and finally (xiii) an Intel Pentium based personal computer for the control of the acquisition and data storage and analysis.

A. Light source and delivery

The Hamamatsu picosecond light pulser (PLP) NIM module is used as the light source. It houses two laser diodes operating at 780 and 830 nm. This device is similar to the Hamamatsu PLP-02 with temperature control and regulated drive circuit. The typical average power at the end of the delivery fiber is ~20 μW for both the wavelengths used. The power employed is within the Food and Drug Administration (FDA) CLASS I standards and no special safety features are required for the operation of the instrument. The pulse repetition rate is 5 MHz and the output light pulse full-width at half-maximum (FWHM) for both diodes is ~50 ps. The two wavelengths are time shared by introducing an electrical delay line between the diode driving circuits (typical 12 ns) and coupled together with a 50/50 fused coupler (OZ optics LTD, Ontario, Canada).

Analysis of time resolved measurements are very sensitive to the initial time t_0 that the pulse was launched into the sample under measurement. For this reason a 95%/5%, 100/140 μm core/clad silica fused coupler from the same company is used, to introduce a reference branch as shown in Fig. 2(a) and monitor the t_0 simultaneously with any measurement. The reference channel can be either coupled alone to the eighth detector leaving seven data channels available or simultaneously with the eighth fiber bundle. The length has been adjusted so the narrow peak does not interfere even with a wide time-resolved curve in the time window. The 95% branch is connected to a DiCon Fiberoptics GP700 1×9 optical switch. The switch can be operated manually or remotely through an IEEE 488.2 port. The switching time is ~0.5 s and the typical insertion loss is 0.6 dB. The 10-m-long multimode graded-index Spectran 100/140 fiber guides are pigtailed to the optical switch. At the other end of the fiber, thin rods made of Delrin® acetal resin were used to create connectors that mount the fiber on the measurement pad.

B. Light detection

The detector used is the R4110U-05 MOD multichannel plate photomultiplier tube (MCP-PMT) from Hamamatsu (NJ). The detector contains 8 MCP detectors in the same package and has very attractive characteristics for photon counting mainly due to the short transient time (TT) and transient time-spread (TTS) features. The eight-channel module is typical of 90 ps TTS per channel. The cross-talk between adjacent channels is of the order of 0.5%. The typical gain at -2700 V (max -2800 *V*) is 10^6 which is similar to most photomultiplier tubes and multichannel plate detectors. The channel to channel gain variation is of the order of 4 dB. The material of the photocathode is extended multialkali with radiant sensitivity (RS) of 15 mA/W at 780 nm and 7 mA/W at 830 nm causing a 3 dB attenuation of the 830 nm signal relative to the 780 nm signal.

The light is delivered to the detectors via eight 1.5-m-long fiber bundles (Hamamatsu NJ). The fiber bundles have an active diameter of 5 mm and are mounted on special to the application pads. Fiber bundles are necessary to ensure delivery of sufficient light for detection. The converted electrical pulses are amplified by 8 C5594 Hamamatsu amplifiers and directed to the photon counting multiplexer and to the SPC-300 photon counting system (Edinburgh Ltd., Edinburgh U.K.). The SPC-300 integrates a complete photon counting system on a single AT-bus card. The system has a minimum time resolution of 18 ps and can effectively count up to 5×10^5 counts due to a fast flash analog-to-digital con-

verter (ADC) in combination with an error-correction technique which allows a virtual 16-bit resolution under such speeds.

C. Instrument impulse response

The FWHM of the instrument's impulse response $h(t)$ is of the order of 200 ps as measured by abutting the source and detector fibers and properly attenuating the signal. The main instrument components that contribute to this finite instrument function are the detector transient time spread (TTS), the photon dispersion along source and detection fibers (~20 ps), the PLP (~50 ps), and the attenuator and photon counting system electronics jitter (~40 ps altogether).

D. Calibration

There is a noticeable amplitude and time delay variation among the channels due to detector gain and fiber guide length variation. Such variations are recorded by measuring the instrument function for all source-detectors combinations. The measurements are made in the presence of the reference channel. All future measurements are being done using the same reference channel in order to be able to correct for laser drift and jitter. Curve fitting the reference channels of the instrument function and data files, with respect to amplitude and time delay, recovers the t_0 at the time of measurement.

E. Laser stability

Three laser operation parameters may have an effect on the accuracy of absorption and scattering calculations. The first two are associated with the pulse launch time drift and random launch time fluctuation or *jitter*. Such phenomena translate to timing differences of the trigger pulse and result in time uncertainties between the data measurements and the instrument function recording. Allowing for 60 min of warm-up times usually eliminates laser drift problems, which can be further corrected by using the reference measurement. However the jitter, which is determined after the warm-up period by monitoring the time position of the time-resolved curves' maximum as a function of time, is always present. The typical jitter of the instrument is of the order of 25 ps at room temperature. This is the timing error we observe between the instrument function measurement and the reference branch reading for repeating the same measurement over time. This time uncertainty is the limiting accuracy factor and has been estimated to induce a $\pm 5\%$ uncertainty of absolute absorption and reduced scattering coefficient calculations.

The third parameter, namely the amplitude instability of the source, is an important error factor for the calculations based on amplitude such as in Eq. (14). Measurements of laser stability have indicated an amplitude repeatability of more than 98% in room temperature for both wavelengths, which allows absorption differences calculation with an error of 5×10^{-4} or less.

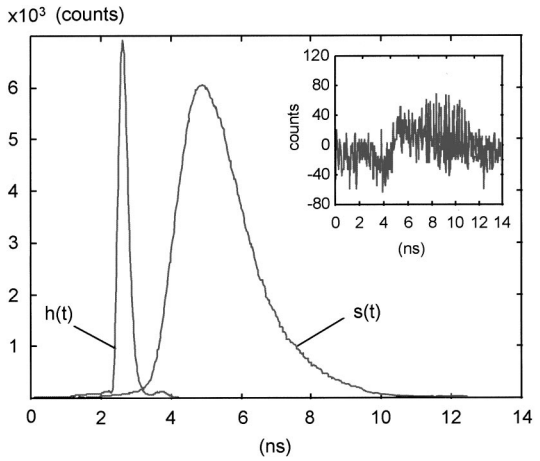

FIG. 3. Time resolved curve $s(t)$ acquired for a source detector separation of 7 cm through 0.5% intralipid solution and the associated instrument function $h(t)$. The inset shows the residual between the measured curve and the result of the fitting process.

IV. EXPERIMENTAL RESULTS

We demonstrate the spectroscopic sensitivity, accuracy, and interchannel variations of the instrument using model measurements. Two types of models were used:

The first type utilizes suspensions of Intralipid (Kabi Pharmacia, Clayton, NC) emulsion and India ink (3080-4 KOH-I-NOOR Inc. Bloomsbury NJ08804) diluted in water in a $40\times50\times60$ cm^3 ''fishtank.'' Intralipid is a polydisperse suspension of fat particles ranging in diameter from 0.1 to 1.1 μm and serves as the scattering background medium. By diluting Intralipid we are able to change the scattering properties of our model. Addition of India ink changes the model absorption. For all measurements we submerge our sources and detectors into the solution using special holders in order to simulate infinite media.

The second type of model we employed were solid molds made of clear casting polyester resin (ETI, Fields Landing, CA). Titanium oxide TiO_2 particles (SIGMA, St. Louis, MO) were suspended in the resin before the addition of catalyst. The particles furnish scattering properties to the model, while the addition of India ink again induces absorption. Therefore we are able to create models resembling specific tissue optical properties.

Figure 3 depicts a typical time-resolved curve through 0.5% intralipid solution for source-detector separation of 7 cm in transmittance geometry and the associated instrument function measurement. The high signal-to-noise ratio obtained in measurements like this allows very good fitting results that render the fitted curve and the real measurement virtually indistinguishable. The inset depicts the residual between the real measurement and the result of the fitting procedure.

A. Absolute absorption measurements

Figure 4(a) shows fitted μ_a and μ_s' values of a single source detector pair submerged into a 0.5% IL solution. The medium absorption changes are induced by adding 2.11 μl of India ink in every liter of 0.5% intralipid solution for every step. The extinction coefficient of the ink is measured

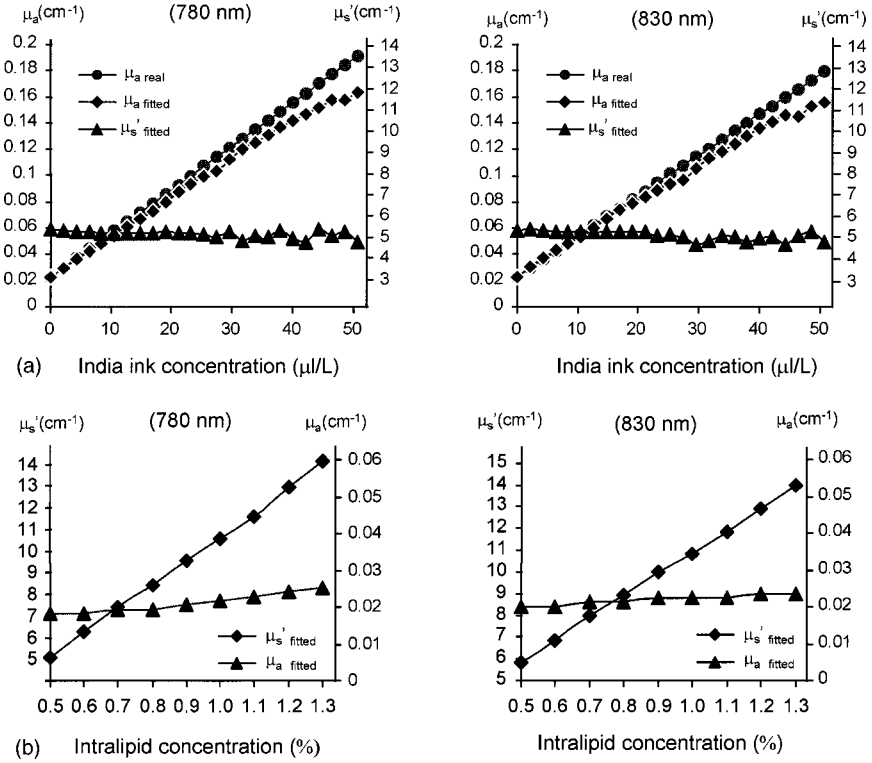

FIG. 4. Experimental spectroscopic data on phantoms. (a) Measurement of absorption and the reduced scattering coefficient as a function of ink concentration in a 0.5% Intralipid-India ink solution at 780 and 830 nm. Real values are calculated from the ink extinction coefficient measured with a spectrophotometer. The observed cross talk between absorption and reduced scattering coefficient may be due to fitting error. (b) Measurement of the reduced scattering coefficient as a function of IL concentration. The background absorption is due to water. Absorption-scattering coefficient cross talk may be again due to fitting error.

in a photospectrometer (Hitachi U2000) and absorption coefficient values are calculated and plotted in the same figure. Both the calculated and fitted absorption values are due to water and ink absorption combined. The range of absorption values was selected to represent absorption properties found in human tissue.[31] The deviation of absolute μ_a values from the theoretically calculated ones, especially in the higher absorption range, arises when the time resolved curve becomes temporally narrower and hence comparable to the instrument function width. Then the fitting procedure becomes more sensitive to convolution, time drift, and jitter errors. The reduced scattering coefficient is also plotted to demonstrate the observed cross-talk of absorption changes to scattering changes. The observed cross-talk may be due to fitting errors.

B. Absolute scattering measurements

Figure 4(b) depicts experimental determination of changes of μ_s' as a function of scatterer concentration. In this experiment concentrated IL (20%) was added incrementally to a 0.5% IL solution in order to vary the scattering properties of the medium from 5 to 13 cm^{-1}. No ink was added. The range of reduced scattering coefficients was similarly selected to be close to the typical values of human breast.[31] Absorption coefficient values are plotted to demonstrate $\mu_a - \mu_s'$ cross-talk in the case of scattering changes. Again the observed cross-talk may be due to fitting error.

C. Quantification of absorption changes

In this experiment intralipid solution was used again to simulate the scattering background at $\mu_s' \sim 5\ cm^{-1}$. A measurement obtained from the solution with no ink added constituted the baseline measurement. Subsequently small quantities of India ink (0.211 μL/L) were added to induce absorption increments of $\Delta\mu_a = 10^{-3}\ cm^{-1}$. Absorption differences between the baseline and the subsequent measurements were calculated using Eq. (16) and the result is shown in Fig. 5 as a function of ink concentration. The experimental data verify the simulated data of Fig. 1. The error of the experimental measurement is approximately double that of the simulation due to issues related with the amplitude stability of the laser.

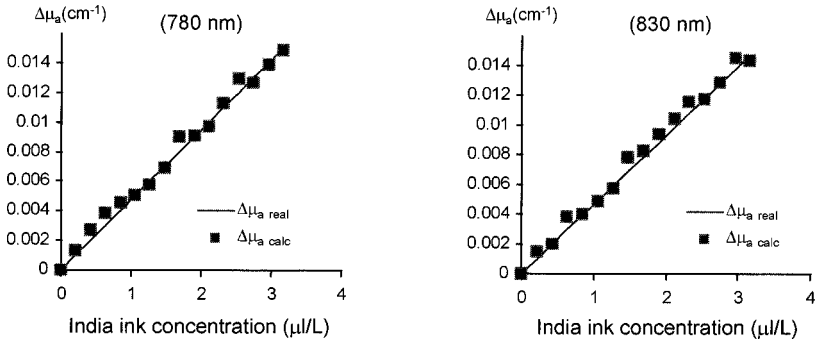

FIG. 5. Measurement of absorption changes using Eq. (14) induced in a 0.5% Intralipid solution, by adding India ink at 780 and 830 nm. Real absorption change values are derived theoretically from the ink extinction coefficient measured with a spectrophotometer.

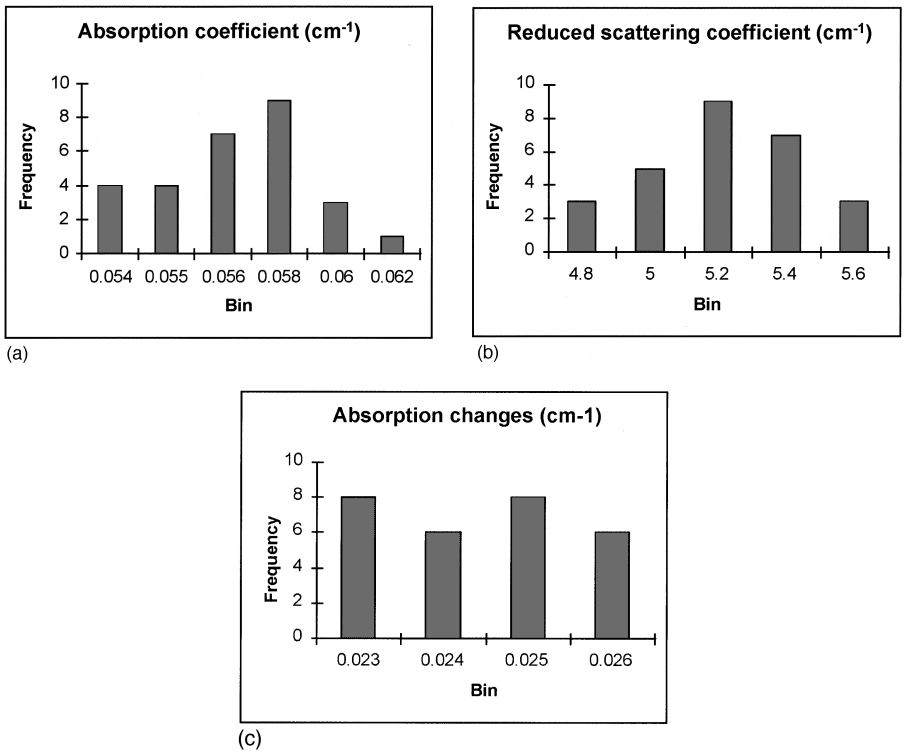

FIG. 6. Interchannel variation (a) Variation of absorption coefficient calculated using Eq. (9) for 7×4 source-detector pairs on a resin model for the 780 nm wavelength. (b) Variation of the reduced scattering coefficient calculated using Eq. (9) for the different pairs employed and the same wavelength and resin model. (c) Interchannel variation in calculating absorption differences using Eq. (14) on measurements from an IL model. Smaller interchannel variation is observed compared to the fitting method. The observed distribution can be mainly attributed to laser amplitude instability. In all cases similar variation is observed for the 830 nm channel.

D. Interchannel variation

In order to examine the interchannel variation we have performed measurements on a homogeneous resin model with $\mu_s = 0.05\ \mathrm{cm}^{-1}$ and $\mu_s' = 8\ \mathrm{cm}^{-1}$ using reflectance geometry, using seven sources and four detectors. Figure 6 depicts the reduced scattering and absorption coefficient distribution calculated for all source-detector pairs used for the 780 nm. Similar behavior is observed for the 830 nm. Interchannel variation is within $\pm5\%$ of the mean calculated value for all channels, and within $\pm3\%$ if only the short separation (and therefore good signal to noise ratio) pairs are considered.

Interchannel variation was also examined when the absorption difference calculation was employed. In this case seven sources and four detectors were employed in a transmittance geometry. The scattering medium was 0.5% Intralipid solution and a 0.01 cm^{-1} absorption change was induced by adding India ink as before. The absorption differences at 780 nm calculated for different channel, are plotted as a histogram in Fig. 6(c). Again no difference in

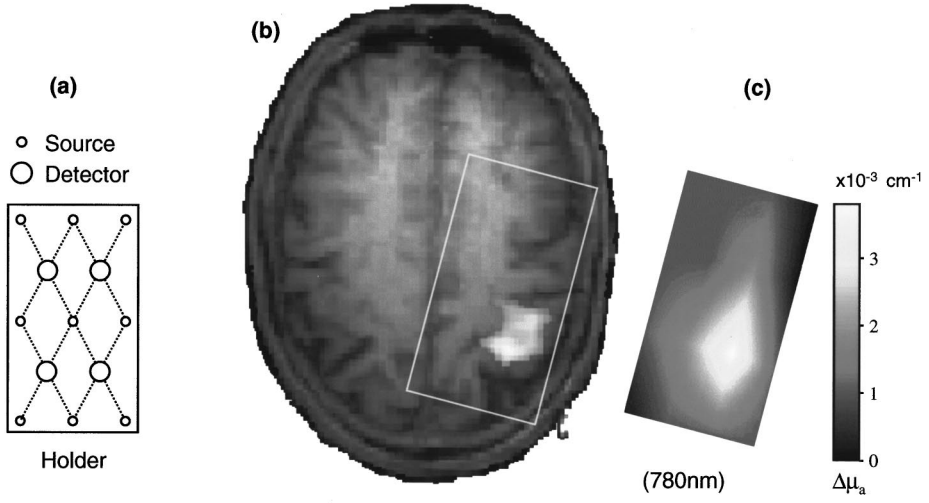

FIG. 7. Application of spatially resolved spectroscopy to monitoring motor cortex activity. (a) Fiber holder used to place nine sources and four detectors on the skull of a healthy volunteer. (b) Functional MRI image of motor cortex activation during finger tapping. (c) Absorption changes map during the same activation protocol, on the same volunteer as in the *f*MRI image. A total of 4×4 spatially resolved spectroscopic measurements are considered which are indicated in (a) with dotted lines. The maximum absorption change coregisters well with the *f*MRI Image.

variability is observed between the 780 and 830 nm. Interchannel variation in this case is below $\pm 2\%$ which can be attributed solely to laser amplitude variations and signal-to-noise ratio.

E. Spatially resolved spectroscopy

In order to illustrate the assessment of spatially resolved spectroscopic measurements we report the use of the instrument in monitoring absorption changes in the contralateral primary motor cortex area occurring due to motor stimulation with voluntary finger tapping. Similar motor-cortex activity is customarily monitored using functional magnetic resonance imaging[32] (*f*MRI) and recently with continuous wave (cw) and phased array (PA) methods.[33,34] However the use of time resolved methods affords more readily the quantification of oxy- and deoxy-hemoglobin.

In this experiment we have used spatially resolved NIR spectroscopy to monitor the activity of the motor cortex of a volunteer and have coregistered it with *f*MRI using the same activation protocol. A specially designed probe, having the geometry shown in Fig. 7(a), was employed to place nine light sources and four photodetectors on the skull of the subject. The activation protocol used is similar to the one reported for cw measurements[35] and consists of a relaxation period of 30 s during which a baseline measurement is obtained and an activation period of 20 s where the activity measurement is obtained. The protocol is repeated for each source. The whole scan sequence lasts 10 min. Tissue optical properties were calculated for the 16 source-detector pairs indicated in Fig. 7(a) with dotted lines. Background absorption and scattering for the 780 nm data were calculated by fitting the solution to the diffusion equation for reflectance geometry to the measurements. Interchannel variation was found to be within the accuracy limits of the instrument, therefore no local tissue variation was assumed at baseline. The average absolute absorption coefficient value was found to be $\mu_a = 0.16\ \mathrm{cm}^{-1}$ and average reduced scattering coefficient $\mu_s' = 12.5\ \mathrm{cm}^{-1}$.

Figure 7(b) shows an axial slice obtained from a layer 2 cm under the surface where the optical probe was placed. Figure 7(c) depicts a 4×4 map of spatially resolved absorption changes between relaxation and activation intervals as calculated using Eq. (16). Each cell of the map corresponds to one source detector pair and indicates the absorption change that occurred in the volume under the respective source-detector pair. Spline interpolation has been employed to enhance the map visual presentation. The whole map corresponds to the area indicated on the *f*MRI image by the solid line. The NIR image illustrated has been interpolated since absorption changes are expected to be gradual between adjacent areas. Coregistration of the optical probe and the MRI image is performed with the use of special water and copper sulfate markers that create anchor points on the MR images. One of these markers can still be seen near the lower, right corner of rectangle marking the position of the optical probe on the *f*MRI image.

The *f*MRI and NIR results are in excellent agreement as to the location of the activation. The difference in the shape of the activation is explained because of the low-resolution spectroscopic map. No significant scattering change is observed. The scattering changes, calculated after fitting the activity measurements and comparing them to the baseline measurements, are within the error limits of the instrument and validate the use of Eq. (16) in our measurements.

F. Discussion

We have demonstrated an efficient instrument for detection and calculation of local optical variations, employing parallel data acquisition of time resolved NIR pulse broadening. The accuracy of the instrument has been shown to be suitable even for small biological signals. Quantification of absolute absorption and reduced scattering coefficients exhibits linear response for the range encountered in biological applications. The error of the absolute quantification has been found to be $\pm 5\%$ and is attributed to laser jitter, photon dispersion in the detection system, experimental uncertainty and theoretical approximations. Quantification of absorption *changes*, under the assumption of invariable scattering background, has been shown to attain sensitivity of the order of $10^{-4}\ \mathrm{cm}^{-1}$ and accuracy of the order of $10^{-3}\ \mathrm{cm}^{-1}$. The limitations here are mainly due to laser instabilities. The high performance of the quantification of absorption changes was successfully applied to quantification of absorption changes during primary motor cortex activity.

ACKNOWLEDGMENTS

We would like to thank Mitsuharu Miwa from Hamamatsu (JP) and Kenneth Kauffman from Hamamatsu (USA) for their technical support. This work was supported by NIH Grant No. CA60182.

[1] E. M. Sevick, B. Chance, J. C. Leigh, S. Nioka, and M. Maris, Anal. Biochem. **195**, 330 (1991).
[2] C. E. Cooper, C. E. Elwell, J. H. Meek, S. J. Matcher, J. S. Wyatt, M. Cope, and D. T. Delpy, Pediatr. Res. **39**, 32 (1996).
[3] C. E. Cooper, M. Cope, V. Quaresima, M. Ferrari, E. Nemoto, R. Springett, S. Matcher, P. Amess, J. Penrice, L. Tyszczuk, J. Wyatt, and D. T. Delpy, Adv. Exp. Med. Biol. **413**, 63 (1997).
[4] S. J. Matcher, M. Cope, and D. T. Delpy, Phys. Med. Biol. **39**, 177 (1994).
[5] D. A. Benaron, W. E. Benitz, R. L. Ariagno, and D. K. Stevenson, Clin. Ped. **31**, 258 (1992).
[6] R. E. Hayden, M. A. Tavill, S. Nioka, T. Kitai, and B. Chance, Head Neck Surgery **122**, 1347 (1996).
[7] D. M. Peebles, A. D. Edwards, J. S. Wyatt, M. Cope, D. T. Delpy, and E. O. Reynold, Am. J. Obst. Gyn. **167**, 1916 (1992).
[8] R. A. De Blasi, I. Alviggi, M. Cope, C. Elwell, and M. Ferrari, Adv. Exp. Med. Biol. **345**, 685 (1994).
[9] T. Binzoni, P. Cerretelli, M. Ferrari, and D. Delpy, Int. J. Sports Med. **18**, 312 (1997).
[10] L. S. L. Arakaki and D. H. Burns, Appl. Spectrosc. **46**, 1919 (1992).
[11] A. Villringer and B. Chance, Trends Neurosci. **20**, 435 (1997).
[12] S. Nioka, Y. Yung, M. Schnall, S. Zhao, S. Orel, C. Xie, B. Chance, and L. Solin, Adv. Exp. Med. Biol. **411**, 227 (1997).
[13] J. M. Conway, K. H. Norris, and C. Bodwell, Am. J. Clin. Nutr. **40**, 1223 (1984).
[14] M. Kohl, M. Essenpreis, and M. Cope, Phys. Med. Biol. **40**, 1267 (1995).
[15] B. Chance, J. S. Leigh, H. Miyake, D. S. Smith, S. Nioka, R. Greenfeld, M. Finander, K. Kaufmann, W. Levy, M. Young, P. Cohen, H. Yoshioka, and R. Boretsky, Proc. Natl. Acad. Sci. USA **85**, 4971 (1988).
[16] J. S. Wyatt, M. Cope, D. T. Delpy, C. E. Richardson, A. D. Edwards, S. Wray, and E. O. Reynolds, J. Appl. Phys. **68**, 1086 (1990).

[17] S. J. Madsen, E. R. Anderson, R. C. Haskell, and B. J. Tromberg, Opt. Lett. **19**, 1934 (1994).
[18] J. B. Fishkin, P. T. C. So, A. E. Cerussi, S. Fantini, M. A. Francheshini, and E. Gratton, Appl. Phys. Lett. **34**, 1143 (1995).
[19] M. S. Patterson, B. Chance, and B. C. Wilson, Appl. Opt. **28**, 2331 (1989).
[20] V. Ntziachristos, X. Ma, and B. Chance, Rev. Sci. Instrum. **69**, 4221 (1998).
[21] A. Ishimaru, *Wave Propagation and Scattering in Random Media* (Academic, New York, 1978).
[22] P. A. Jannson, *Deconvolution with Applications in Spectroscopy* (Academic, Orlando, 1984).
[23] P. A. Jannson, R. H. Hunt, and E. K. Plyler, J. Opt. Soc. Am. **60**, 596 (1970).
[24] P. H. Van Cittert, Z. Phys. **69**, 298 (1931).
[25] B. R. Frieden, J. Opt. Soc. Am. **62**, 511 (1972).
[26] B. R. Frieden, *Probability, Statistical Optics, and Data Testing* (Springer, New York, 1983).
[27] D. W. Marquardt, J. Soc. Ind. Appl. Math. **11**, 431 (1963).
[28] W. H. Press, B. P. Flannery, S. A. Teukolsky, and W. T. Vetterling, *Numerical Recipes in C: The Art of Scientific Computing* (Cambridge University Press, New York, 1988).
[29] R. C. Haskel, T. Svaasand, T. Tsay, T. Feng, M. S. McAdams, and B. J. Tromberg, J. Opt. Soc. Am. A **11**, 2727 (1994).
[30] T. J. Farell, M. S. Patterson, and B. Wilson, Med. Phys. **19**, 879 (1992).
[31] W. F. Cheong, S. A. Prahl, and A. J. Welch, IEEE J. Quantum Electron. **26**, 2166 (1990).
[32] Proceedings of the International Society of Magnetic Resonance, Vancouver, Canada, 1997.
[33] A. Villringer and B. Chance, Trends Neurosci. **20**, 435 (1997).
[34] B. Chance, Q. Luo, S. Nioka, D. C. Alsop, and J. A. Detre, Philos. Trans. R. Soc. London, Ser. B **352**, 707 (1997).
[35] H. Obrig, C. Hirth, J. Junge-Hülsing, C. Döge, T. Wolf, U. Dirnagl, and J. Villringer, Appl. Phys. **81**, 1174 (1996).